Surface tension of the two center Lennard-Jones plus point dipole fluid

Stephan Werth,[1] Martin Horsch,[1, a)] and Hans Hasse[1]

Laboratory of Engineering Thermodynamics, Department of Mechanical and Process Engineering, University of Kaiserslautern, Erwin-Schrödinger-Str. 44, 67663 Kaiserslautern, Germany

Molecular dynamics simulations are used for systematically studying the surface tension of the two center Lennard-Jones plus point dipole (2CLJD) model fluid. In a dimensionless representation this model fluid has two parameters describing the elongation and the dipole moment. These parameters were varied in the entire range relevant for describing real fluids resulting in a grid of 38 individual models. For each model the surface tension was determined at temperatures between 60 and 90 % of the critical temperature. For completeness, also the vapor pressure and the saturated densities were determined. The latter results agree well with literature data, whereas for the surface tension only few data were previously available. From the present results, an empirical correlation for the surface tension of the 2CLJD model as a function of the model parameters is developed. The correlation is used to predict the surface tension of 46 2CLJD molecular models from the literature, which were adjusted to bulk properties, but not to interfacial properties. The results are compared to experimental data. The molecular models overestimate the surface tension, and deviations between the predictions and experimental data are below 12 % on average.

Keywords: Molecular simulation, Surface tension, Lennard-Jones potential, Dipole, Stockmayer fluid

[a)] Author to whom correspondence should be addressed: martin.horsch@mv.uni-kl.de

I. INTRODUCTION

The two center Lennard-Jones plus point dipole (2CLJD) class of molecular models is widely used for describing refrigerants and carbon monoxide[1–9]. It is a generalization of the Stockmayer fluid[10] which also takes the shape of the molecule into account. There are several molecular models of the 2CLJD type in the literature for R22[1,2,6], R23[1,6], R32[1,6], R125[1,6], R134a[1,3,4,6], R142b[1,4,6], R142a[4,6] and R152a[1,2,4–6]. Stoll et al.[6] developed 46 2CLJD molecular models for dipolar fluids including carbon monoxide as well as methane, ethane and ethene derivatives. These models were adjusted to the saturated liquid density and the vapor pressure[6], which they usually describe with deviations below 1 % and 5 %, respectively. For simulating 2CLJD models, instead of the point dipole also two point charges of opposite sign can be used, if they are suitably placed[11].

In previous work a systematic evaluation of the surface tension of the two center Lennard-Jones plus point quadrupole (2CLJQ) molecular model class was conducted[12]. These models, on average, overestimate surface tension by about 20 %[13]. Other molecular models which have been adjusted to bulk properties, but not to interfacial properties, exhibit a similar deviations[13–24]. Embedded-atom force fields for metals, however, tend to underestimate the vapor-liquid surface tension[25]. Another theoretical method for the prediction of the surface tension is the density functional theory in combination with an equation of state[26–31]. Thereby, an empirical correction expression is often employed, which is attributed to the presence of capillary waves and decreases the surface tension. Without this correction term, which was adjusted to fit the experimental surface tension values of the n-alkane series[26], density functional theory would deviate from the surface tension of real fluids in a similar way as the molecular models mentioned above.

Bulk properties of the vapor-liquid equilibrium (VLE) of the 2CLJD model fluid have been studied systematically in the literature[6,32]. These results have been used for the development of the dipolar contribution to the PCP-SAFT equation of state[33]. Also Joule-Thomson coefficients[34] and transport properties[35,36] of the 2CLJD fluid are available.

There are also studies of the surface tension of the 2CLJD fluid[37–39], but no systematic evaluation regarding the influence of the molecular model parameters was performed so far. In the present work, a systematic study on the surface tension of 2CLJD molecular models is conducted, covering the entire parameter range of literature models for real fluids

which were previously described by that model. The results can be used for predicting the surface tension of 2CLJD models or for the parameterization of 2CLJD models using surface tension data from experiments. They are used here for predicting the surface tension of 2CLJD models which were previously developed in our group[6], and comparing the results to experimental data.

II. SIMULATION METHOD

The molecular models studied in the present work are rigid and consist of two identical Lennard-Jones (LJ) sites, a distance L apart from each other, and a point dipole in the center of mass. The LJ potential is described by

$$u_{ij}^{\mathrm{LJ}} = 4\epsilon \left[\left(\frac{\sigma}{r_{ij}} \right)^{12} - \left(\frac{\sigma}{r_{ij}} \right)^{6} \right], \tag{1}$$

with the size and energy parameters σ and ϵ. The dipole-dipole interaction is described by

$$u_{ij}^{\mathrm{D}} = \frac{1}{4\pi\epsilon_0} \frac{\mu_i \mu_j}{r_{ij}^3} f(\omega), \tag{2}$$

where ϵ_0 is the electric constant, μ_i and μ_j are the dipole moments of the molecules, and $f(\omega)$ is a dimensionless angle-dependent expression[40].

For the present series of molecular dynamics simulations, systems were considered where the vapor and liquid phases coexist with each other in direct contact, employing periodic boundary conditions, so that there are two vapor-liquid interfaces which are oriented perpendicular to the y axis. The surface tension was computed from the deviation between the normal and the tangential diagonal components of the overall pressure tensor[41,42]

$$\gamma = \frac{1}{2A} \left(\Pi_N - \Pi_T \right) = \frac{1}{2} \int_{-\infty}^{\infty} \mathrm{d}y \left(p_N - p_T \right). \tag{3}$$

Thereby, the normal pressure p_N is given by the y component of the diagonal of the pressure tensor, and the tangential pressure p_T was determined by averaging over x and z components of the diagonal of the pressure tensor. The surface area A of each vapor-liquid interface is given by the cross section of the simulation volume normally to the y axis.

All thermodynamic properties can be reduced by the LJ parameters σ and ϵ, the mass m, as well as the Boltzmann constant k_B. Furthermore, the convention $4\pi\epsilon_0 = 1$ is employed here to simplify the expressions involving dipole moments.

This approach reduces the parameters of the 2CLJD fluid to two: the reduced elongation L/σ and the reduced dipole strength $\mu^2/\epsilon\sigma^3$. An overview of the 38 parameter combinations for which simulations were carried out in the present study is given in Fig. 1. Parameter values of 2CLJD models of real fluids from the literature[1–6] are also indicated in Fig. 1. The temperature was varied from 60 to 90 % T_c, where T_c is the critical temperature, which is estimated here by the equation of Stoll et al.[32].

Zubillaga et al.[23] pointed out that a proper treatment of the long-range interactions has a strong influence on the predicted surface tension values[43–46]. This treatment can be either done by brute-force simulations with very large cutoff radii of the order of 10 molecular segment diameters[23,47–50], which are very time consuming, or by using asymmetric long range corrections for the dispersive and electrostatic interactions. A large variety of long range corrections methods exist, ranging from MMM type algorithms[51], scaling with $\mathcal{O}\left(N^2\right)$ in terms of the particle number N, Ewald summation techniques[52–54], with $\mathcal{O}\left(N^{3/2}\right)$ or $\mathcal{O}\left(N\log N\right)$ scaling, to slab-based long range corrections based on the density profile with a more favorable linear scaling, i.e. $\mathcal{O}\left(N\right)$[55–57]. In the present work, the cutoff radius was set to 5 σ and a center-of-mass cutoff scheme was employed. The Lennard-Jones interactions were corrected with a slab-based long range correction based on the density profile[55]. Electrostatic long-range interactions were approximated by a resulting effective molecular dipole and corrected with a slab-based long range correction based on the density profile[56].

The simulations were performed with the molecular dynamics code *ls1 mardyn*[58,59] in the canonical ensemble with N = 16,000 particles. The equation of motion was solved by a leapfrog integrator[60] with a time step of $\Delta t = 0.001\ \sigma\sqrt{m/\epsilon}$. The elongation of the simulation volume normal to the interface was 80 σ and the thickness of the liquid film in the center of the simulation volume was 40 σ to account for finite size effects[61]. The elongation in the other spatial directions was at least 20 σ. The equilibration was executed for 500,000 time steps. The production was conducted for 2,500,000 time steps to reduce statistical uncertainties. The statistical errors were estimated to be three times the standard deviation of five block averages, each over 500,000 time steps. The saturated densities and vapor pressures were calculated as an average over the respective phases excluding the area

close to the interface, i.e. the area where the first derivative of the density with respect to the y coordinate deviated from zero significantly.

III. RESULTS AND DISCUSSION

A. Model fluids

Table I shows the results for the vapor pressure p^{S}, the saturated liquid density $\rho^{'}$, the saturated vapor density $\rho^{''}$ and the surface tension γ obtained for the 38 2CLJD model fluids.

Stoll et al.[32] used the NpT + test particle method[62,63] for determining the saturated densities and the vapor pressure of the same 38 model fluids. Figs. 2 and 3 show correlations of the data of Stoll et al.[32] compared to the simulation results from the present work. The deviations between the present simulation results and the correlations are within the statistical uncertainties in all cases.

The results for the surface tension of the 2CLJD model fluids are shown in Fig. 4 as a function of the temperature for three different dipole moments and six different elongations. The surface tension increases with an increasing dipole moment and decreases with an increasing elongation. This result is similar to the result for the 2CLJQ model fluid[12]. Fig. 5 shows the surface tension of the 2CLJD model at 70 % of the critical temperature as a function of the elongation and the dipole moment. This temperature is commonly used for corresponding-states methods[64,65]. Similiar to results in Fig. 4, the surface tension at 70 % of the critical temperature increases with an increasing dipole moment and decreases with an increasing elongation.

Following the principle of corresponding states[64,65], the surface tension is correlated here using a critical scaling expression

$$\gamma = A \left(1 - \frac{T}{T_c}\right)^B \epsilon\sigma^{-2}. \tag{4}$$

The critical temperature is calculated with the correlation of Stoll et al.[6]. Functions for A and B are fitted simultaneously to all simulation results from the present work, adopting the approach of Stoll et al.[12,66]. It turns out that for obtaining a good correlation A should depend both on μ and L, whereas it is sufficient to have B as a function of μ only. The

functional forms are as follows:

$$A\left(\mu^2/\epsilon\sigma^3, L/\sigma\right) = a + \sum_{i=1,2} b_i \left(\mu^2/\epsilon\sigma^3\right)^i + c\,(L/\sigma)^2/\left((L/\sigma)^2 + f\right)$$
$$+ \sum_{i=1,2} d_i \left(\mu^2/\epsilon\sigma^3\right)^i/\left((L/\sigma)^2 + f\right) + e\,\mu^2/\epsilon\sigma^3 (L/\sigma)^2/\left((L/\sigma)^2 + f\right), \quad (5)$$

$$B\left(\mu^2/\epsilon\sigma^3\right) = \alpha + \beta\,\mu^2/\epsilon\sigma^3. \quad (6)$$

The parameters of Eqs. (5) and (6) are given in Table II. The correlation generally agrees with the simulation data within their statistical uncertainties, cf. Figs. 4 and 6. The relative deviations between the simulation data and the correlation are given in Fig. 6. The relative mean deviation between the simulation data and the correlation is 2.2 %. This deviation is significantly below the relative statistical uncertainty, which is 8 % on average.

Fig. 7 shows a comparison of the results from the present work with literature results on the surface tension of 2CLJD fluids. The results from Enders et al.[39] and Mecke et al.[38] were calculated using a large cutoff radius for the LJ potential and an Ewald summation for the dipolar interactions. Moore et al.[37] used an Ewald summation for the dispersive and dipolar interaction. The results from the present work and those from Moore et al.[37] and Mecke et al.[38] are in very good agreement with each other. The results from Enders et al.[39] are slightly below the results from the present work. This might be due to the truncation of the LJ potential, i.e. the absence of a long range correction for dispersive interactions in the simulations by Enders et al.[39], as opposed to the present work.

B. Application to real fluids

Table III shows the parameters of the molecular models for real fluids by Stoll et al.[6] The deviations $\delta\rho'$ and δp^{S} are taken from Stoll et al.[6] and represent relative mean deviations of the simulations results from experimental data. The relative mean deviation $\delta\gamma$ is calculated in a similar manner. It represents the relative deviation of the predicted surface tension for the 2CLJD molecular models by Eq. (4) from DIPPR correlations to experimental data from 55 % to 95 % of the critical temperature. Both the DIPPR correlations and the correlations of the simulation data are subject to errors, which are 3 %[67] and 2.2 % respectively. In the case of R161 the DIPPR correlation does not match the experimental data[68,69] and the

correlation parameters from Mulero et al. are used instead[68].

In the case of 12 fluids - R12B1, R30B1, R40B1, R41, R112a, R123B1, R131b, R1113B1, R1122, R1132a, R1140, R1141 - no experimental data are available at all. The DIPPR correlation is a prediction based on the parachor method[70,71], where the parachor was estimated based on the molecular structure[67,72]. The results are given in parentheses in Table III.

Figs. 8, 9, 10 and 11 show the surface tension over the temperature for methane, ethane, ethene derivatives and carbon monoxide. The molecular models were not adjusted to reproduce the surface tension, which is thus strictly predictive.

The surface tension of the molecular models by Stoll et al.[6] agrees reasonably well with experimental data. The molecular models match the critical point in all cases within 3 K[6]. The surface tension is in most cases overestimated by the molecular models, which was also found for the 2CLJQ molecular models[13]. On average the deviation between the prediction by the molecular models and the DIPPR correlations is 11.9 %. This agreement is slightly better than the predictions made by the 2CLJQ molecular model class where an average deviation of 20 % from experimental data for the surface tension was found[13].

Fig. 12 shows the histogram of the relative deviation contribution of the surface tension of the 2CLJD models from experimental data. Over two thirds of the molecular models show a deviation below 15 % in the surface tension.

For completeness the comparison between the model predictions and the DIPPR correlation which are not based on experimental data but on an estimation using the parachor method are shown in Fig. 1 of the supplementary material. In some cases very high deviations (up to 72 % for R30B1) are observed, even though molecular models for chemically similar fluids showed a very good agreement with experimental data, e.g. R10B1 (2.5 %), R12B1 (5.0 %), R23 (18.3 %), R32 (10.8 %). In Fig. 13 predictions are shown for the molecular simulation, the DIPPR correlation based on the parachor method as well as a group contribution method by Rarey et al.[73], which is implemented in the Dortmund Data Bank. The results from the method by Rarey et al. compare favorably to the molecular simulation, whereas the predictions by the DIPPR correlations are far off. These results cast doubts on the prediction of the surface tension based on the parachor method.

IV. CONCLUSION

In the present work, the surface tension of the 2CLJD fluid was systematically evaluated by molecular dynamics simulation. Based on literature models for real fluids, the dimensionless parameters were varied in the entire range that is relevant for real fluids. A correlation expression was deduced that accurately describes the complex relation between the surface tension and the molecular model parameters.

In particular, the surface tension was evaluated for the 46 molecular models by Stoll et al.[6], which were parameterized to reproduce the saturated liquid density and the vapor pressure. The deviation between the predictions by these molecular models and experimental data for the surface tension of real fluids is about 12 % on average. These deviations are not large considering the errors of the experimental and simulation data on which they rely. To improve the molecular models for the surface tension, the respective experimental data have to be taken into account during the model development, e.g. by multi-criteria optimization on the basis of an analysis of the Pareto set[13,74,75].

ACKNOWLEDGEMENT

The authors gratefully acknowledge financial support from BMBF within the SkaSim project (grant no. 01H13005A) and from Deutsche Forschungsgemeinschaft (DFG) within the Collaborative Research Center (SFB) 926. They thank Patrick Leidecker for performing some of the present simulations and Andreas Köster, Jadran Vrabec and Jürgen Rarey for fruitful discussions. The present work was conducted under the auspices of the Boltzmann-Zuse Society of Computational Molecular Engineering (BZS) and the simulations were carried out on the Regional University Computing Center Kaiserslautern (RHRK) under the grant TUKL-MSWS as well as on JUQUEEN at Jülich Supercomputing Center under the grant HKL09 within the PARSIVAL scientific computing project.

REFERENCES

[1]G. Gao, W. Wang, and X. C. Zeng. *Fluid Phase Equilib.*, 137:87–98, 1997.

[2]C. Kriebel, M. Mecke, M. Winkelmann, J. Vrabec, and J. Fischer. *Fluid Phase Equilib.*, 142:15–32, 1998.

[3]M. Lísal, R. Budinský, and V. Vacek. *Fluid Phase Equilib.*, 135:193–207, 1997.

[4]M. Lísal, R. Budinský, V. Vacek, and K. Aim. *Int. J. Thermophys.*, 20:163–174, 1999.

[5]C. Vega, B. Saager, and J. Fischer. *Mol. Phys.*, 68(5):1079–1093, 1989.

[6]J. Stoll, J. Vrabec, and H. Hasse. *J. Chem. Phys.*, 119(21):11396–11407, 2003.

[7]M. E. van Leeuwen. *Fluid Phase Equilib.*, 99:1–18, 1994.

[8]B. J. Berne and G. D. Harp. *Adv. Chem. Phys.*, 17:63–227, 1970.

[9]J. O. Hirschfelder, C. F. Curtiss, and R. B. Bird. *Molecular Theory of Gases and Liquids*. Wiley & Sons, New York, 1964.

[10]W. H. Stockmayer. *J. Chem. Phys.*, 9(5):398–402, 1941.

[11]C. Engin, J. Vrabec, and H. Hasse. *Mol. Phys.*, 109:1975–1982, 2011.

[12]S. Werth, M. Horsch, and H. Hasse. *Fluid Phase Equilib.*, 392:12–18, 2015.

[13]S. Werth, K. Stöbener, P. Klein, K.-H. Küfer, M. Horsch, and H. Hasse. *Chem. Eng. Sci.*, 121:110–117, 2015.

[14]J.-C. Neyt, A. Wender, V. Lachet, and P. Malfreyt. *J. Phys. Chem. B*, 115(30):9421–9430, 2011.

[15]S. Eckelsbach, S. Miroshnichenko, G. Rutkai, and J. Vrabec. In W. E. Nagel, D. B. Kröner, and M. M. Resch, editors, *High Performance Computing in Science and Engineering '13*, pages 635–646. Springer, Berlin/Heidelberg, 2013.

[16]J.-C. Neyt, A. Wender, V. Lachet, and P. Malfreyt. *J. Phys. Chem. C*, 116(19):10563–10572, 2012.

[17]C. Avendaño, T. Lafitte, A. Galindo, C. S. Adjiman, G. Jackson, and E. A. Müller. *J. Phys. Chem. B*, 115(38):11154–11169, 2011.

[18]C. Avendaño, T. Lafitte, C. S. Adjiman, A. Galindo, E. A. Müller, and G. Jackson. *J. Phys. Chem. B*, 117(9):2717–2733, 2013.

[19]C. Herdes, T. S. Totton, and E. A. Müller. *Fluid Phase Equilib.*, 406:91–100, 2015.

[20]N. Ferrando, V. Lachet, J. Pérez-Pellitero, A. D. Mackie, and P. Malfreyt. *J. Phys. Chem. B*, 115(36):10654–10664, 2011.

[21]S. Eckelsbach and J. Vrabec. *Phys. Chem. Chem. Phys.*, 17(40):27195–27203, 2015.

[22]S. K. Singh, A. Sinha, G. Deo, and J. K. Singh. *J. Phys. Chem. C*, 113(17):7170–7180, 2009.

[23]R. A. Zubillaga, A. Labastida, B. Cruz, J. C. Martinez, E. Sanchez, and J. Alejandre. *J. Chem. Theory Comput.*, 9(3):1611–1615, 2013.

[24]C. Caleman, P. J. van Maaren, M. Hong, J. S. Hub, L. T. Costa, and D. van der Spoel. *J. Chem. Theory Comput.*, 8(1):61–74, 2012.

[25]J. R. Vella, F. H. Stillinger, A. Z. Panagiotopoulos, and P. G. Debendetti. *J. Phys. Chem. B*, 119(29):8960–8968, 2015.

[26]J. Gross. *J. Chem. Phys.*, 131:204705, 2009.

[27]F. Llovell, A. Galindo, F. J. Blas, and G. Jackson. *J. Chem. Phys.*, 133:024704, 2010.

[28]M. M. Telo da Gama. *Mol. Phys.*, 62(3):585–604, 1987.

[29]P. I. Teixeira and M. M. Telo da Gama. *J. Phys.: Condens. Matter*, 3(1):111–125, 1991.

[30]J. Winkelmann. *J. Phys.: Condens. Matter*, 13(21):4739–4768, 2001.

[31]P. Frodl and S. Dietrich. *Phys. Rev. E*, 48(5):3741–3759, 1993.

[32]J. Stoll, J. Vrabec, and H. Hasse. *Fluid Phase Equilib.*, 209(1):29–53, 2003.

[33]J. Gross and J. Vrabec. *AIChE J.*, 52(3):1194–1204, 2006.

[34]J. Vrabec, G. K. Kedia, and H. Hasse. *Cryogenics*, 45:253–258, 2005.

[35]G. A. Fernandez, J. Vrabec, and H. Hasse. *Fluid Phase Equilib.*, 249:131–139, 2006.

[36]G. A. Fernandez, J. Vrabec, and H. Hasse. *Cryogenics*, 46:711–717, 2006.

[37]S. G. Moore, M. J. Stevens, and G. S. Grest. *Phys. Rev. E*, 91:022309, 2015.

[38]M. Mecke, J. Fischer, and J. Winkelmann. *J. Chem. Phys.*, 114(13):5842–5852, 2001.

[39]S. Enders, H. Kahl, M. Mecke, and J. Winkelmann. *J. Mol. Liq.*, 115(1):29–39, 2004.

[40]C. G. Gray and K. E. Gubbins. *Theory of Molecular Fluids, Vol. 1: Fundamentals*. Clarendon Press, Oxford, 1984.

[41]J. P. R. B. Walton, D.-J. Tildesley, J. S. Rowlinson, and J. R. Henderson. *Mol. Phys.*, 48(6):1357–1368, 1983.

[42]J. G. Kirkwood and F. P. Buff. *J. Chem. Phys.*, 17(3):338–343, 1949.

[43]F. Goujon, P. Malfreyt, and D.-J. Tildesley. *J. Chem. Phys.*, 140:244710, 2014.

[44]S. Werth, M. Horsch, J. Vrabec, and H. Hasse. *J. Chem. Phys.*, 142:107101, 2015.

[45]F. Goujon, P. Malfreyt, and D.-J. Tildesley. *J. Chem. Phys.*, 142:107102, 2015.

[46]F. Goujon, A. Ghoufi, P. Malfreyt, and D.-J. Tildesley. *J. Chem. Theory Comput.*, 11(10):4573–4585, 2015.

[47]O. Lobanova, C. Avendaño, T. Lafitte, E. A. Müller, and G. Jackson. *Mol. Phys.*, 113(9-10):1228–1249, 2015.

[48]D. Duque and L. F. Vega. *J. Chem. Phys.*, 121(17):8611–8617, 2004.

[49]H. Wang, C. Schüte, and P. Zhang. *Phys. Rev. E*, 86:026704, 2012.

[50]G. Galliero, M. M. Piñeiro, B. Mendiboure, C. Miqueu, T. Lafitte, and D. Bessieres. *J. Chem. Phys.*, 130:104704, 2009.

[51]A. Arnold and C. Holm. *J. Chem. Phys.*, 123:144103, 2005.

[52]P. J. in 't Veld, A. E. Ismail, and G. S. Grest. *J. Chem. Phys.*, 127:144711, 2007.

[53]R. E. Isele-Holder, W. Mitchell, and A. E. Ismail. *J. Chem. Phys.*, 137:174107, 2012.

[54]R. E. Isele-Holder, W. Mitchell, J. R. Hammond, A. Kohlmeyer, and A. E. Ismail. *J. Chem. Theory Comput.*, 9(12):5412, 2013.

[55]S. Werth, G. Rutkai, J. Vrabec, M. Horsch, and H. Hasse. *Mol. Phys.*, 112(17):2227–2234, 2014.

[56]S. Werth, M. Horsch, and H. Hasse. *Mol. Phys.*, 113(23):3750–3756, 2015.

[57]J. Janeček. *J. Phys. Chem. B*, 110(12):6264–6269, 2006.

[58]C. Niethammer, S. Becker, M. Bernreuther, M. Buchholz, W. Eckhardt, A. Heinecke, S. Werth, H.-J. Bungartz, C. W. Glass, H. Hasse, J. Vrabec, and M. Horsch. *J. Chem. Theory Comput.*, 10(10):4455–4464, 2014.

[59]W. Eckhardt, A. Heinecke, R. Bader, M. Brehm, N. Hammer, H. Huber, H.-G. Kleinhenz, J. Vrabec, H. Hasse, M. Horsch, M. Bernreuther, C. W. Glass, C. Niethammer, A. Bode, and H.-J. Bungartz. *Supercomputing - XXVIII. International Supercomputing Conference (ISC 2013)*, volume 7905 of *LNCS*, pages 1–12. Springer, Heidelberg, 2013.

[60]D. Fincham. *Mol. Sim.*, 8(3-5):165–178, 1992.

[61]S. Werth, S. V. Lishchuk, M. Horsch, and H. Hasse. *Physica A*, 392(10):2359–2367, 2013.

[62]D. Möller and J. Fischer. *Mol. Phys.*, 69(3):463–473, 1990.

[63]D. Möller and J. Fischer. *Fluid Phase Equilib.*, 100:35–61, 1994.

[64]A. Mejía, C. Herdes, and E. A. Müller. *Ind. Eng. Chem. Res.*, 53(10):4131–4141, 2014.

[65]G. Galliero. *J. Chem. Phys.*, 133:074705, 2010.

[66]J. Stoll, J. Vrabec, H. Hasse, and J. Fischer. *Fluid Phase Equilib.*, 179:339–362, 2001.

[67]R. L. Rowley, W. V. Wilding, J. L. Oscarson, Y. Yang, N. A. Zundel, T. E. Daubert, and R. P. Danner. *DIPPR Information and Data Evaluation Manager for the Design Institute for Physical Properties*. AIChE, 2013. Version 7.0.0.

[68]A. Mulero, I. Cachadina, and M. I. Parra. *J. Phys. Chem. Ref. Data*, 41:043105, 2012.

[69]J. Fan, X. Zhao, and Z. Guo. *Fluid Phase Equilib.*, 316:98–101, 2012.

[70]S. Sugden. *J. Chem. Soc.*, 125:1177–1189, 1924.

[71]D. B. Macleod. *Transact. Faraday Soc.*, 19:38–41, 1923.

[72]T. A. Knotts, W. V. Wilding, J. L. Oscarson, and R. L. Rowley. *J. Chem. Eng. Data*, 46(5):1007–1012, 2001.

[73]*DDB - Dortmund Data Bank*. 7.3.0.458 (DDB), 1.18.0.122 (Artist). DDBST GmbH, Oldenburg, 2015.

[74]K. Stöbener, P. Klein, S. Reiser, M. Horsch, K.-H. Küfer, and H. Hasse. *Fluid Phase Equilib.*, 373:100, 2014.

[75]K. Stöbener, P. Klein, M. Horsch, K.-H. Küfer, and H. Hasse. *Fluid Phase Equilib.*, in press, 2015. DOI:10.1016/j.fluid.2015.11.028.

FIGURES

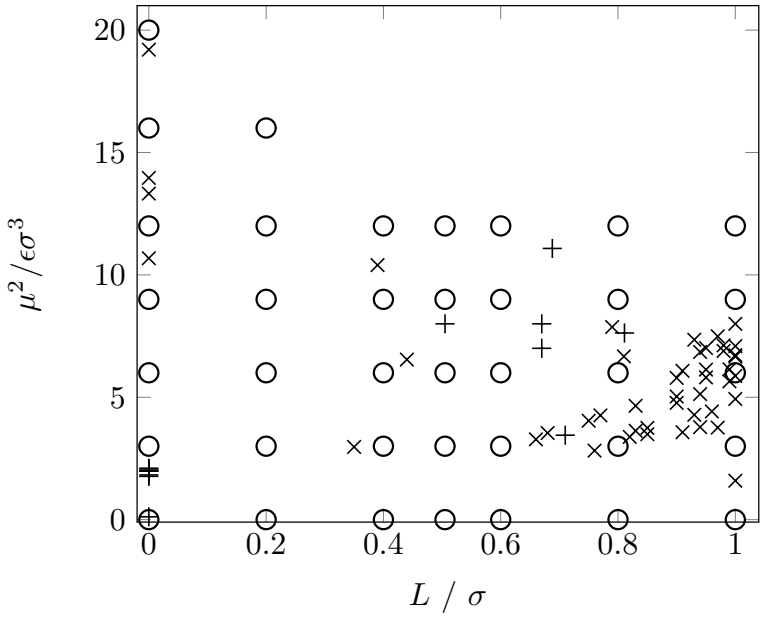

FIG. 1. Reduced parameters of the simulated 2CLJD model fluids: models studied in the present work (o), molecular models by Stoll et al. $(\times)$[6] and other literature models $(+)$[1–5].

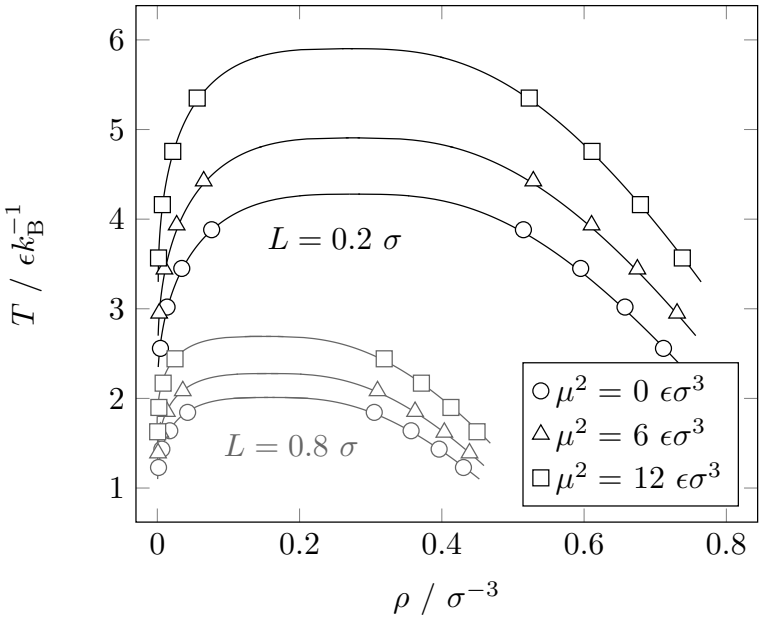

FIG. 2. Saturated densities of the 2CLJD model fluid, including the 2CLJ case (without a dipole). The symbols are the simulation results from the present work. The lines are correlations from Stoll et al.[32]. The simulation uncertainties are smaller than the symbol size in all cases.

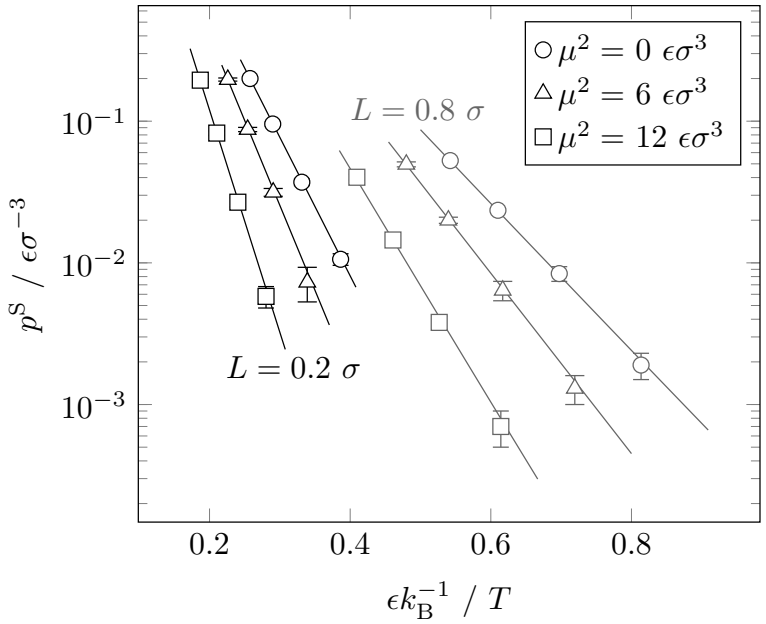

FIG. 3. Vapor pressure curves of the 2CLJD model fluid, including the 2CLJ case (without a dipole). The symbols are simulation results from the present work. The lines are correlations from Stoll et al.[32].

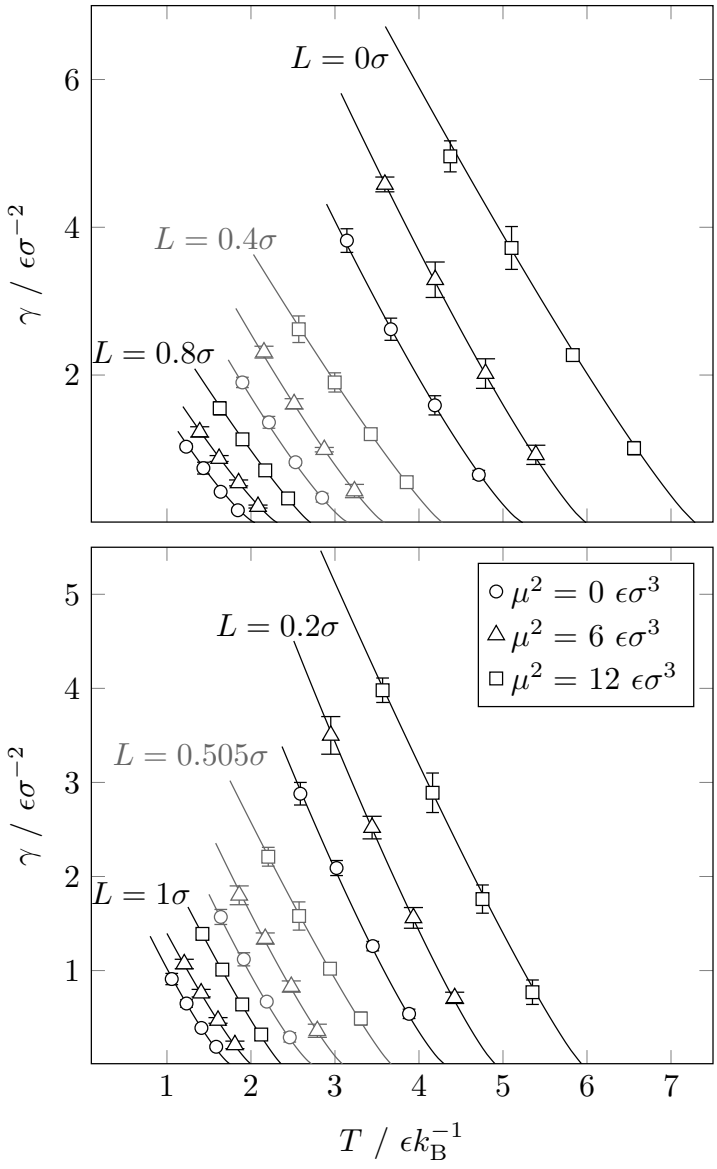

FIG. 4. Surface tension of 2CLJD model fluids over the temperature, including the 2CLJ case (without a dipole) as well as the Stockmayer fluid (without elongation). The symbols are simulation results from the present work. The lines represent the correlation given in Eq. (4).

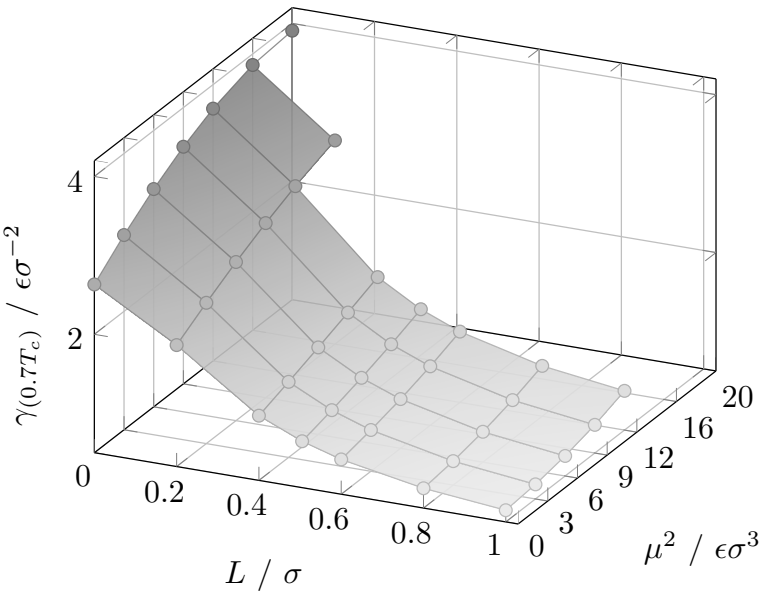

FIG. 5. Surface tension of 2CLJD fluids at 70 % of the critical temperature. The surface represents the correlation given in Eq. (4). The symbols represent the 38 molecular models considered in the present work.

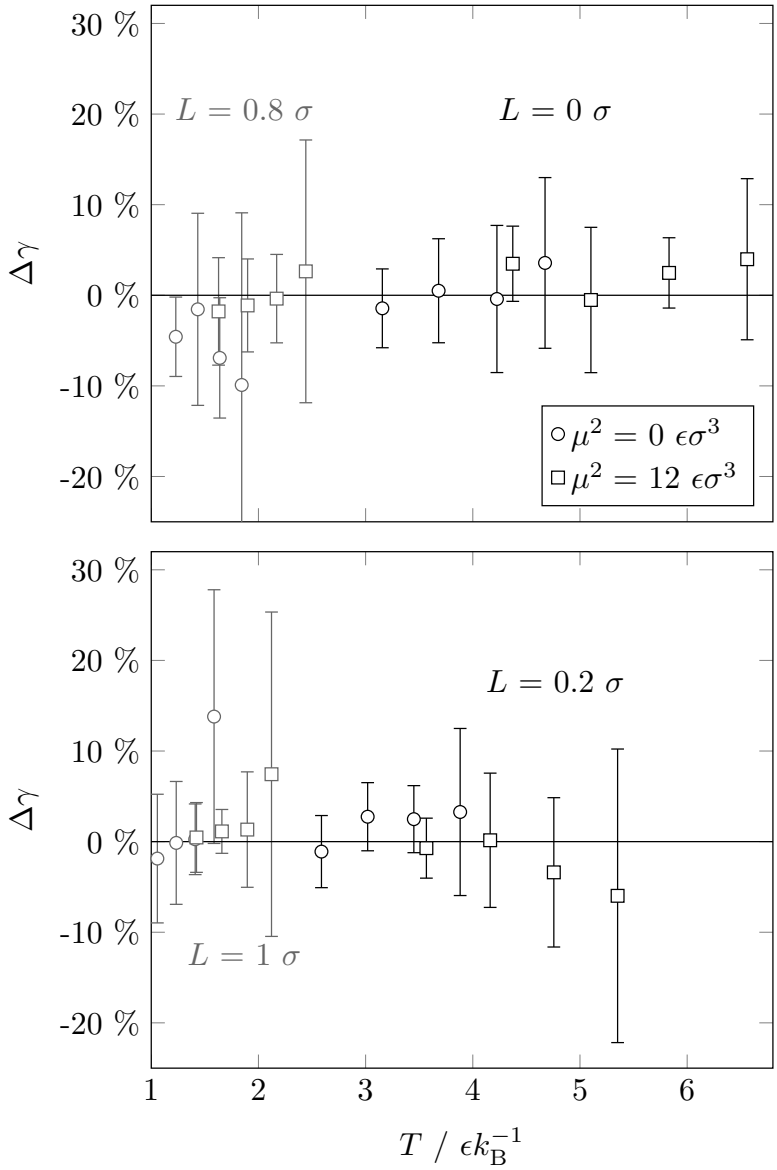

FIG. 6. Relative deviation $\Delta\gamma = (\gamma_\mathrm{corr} - \gamma_\mathrm{sim})/\gamma_\mathrm{sim}$ of simulation results for the surface tension of the 2CLJD model fluid from the correlation given by Eq. (4).

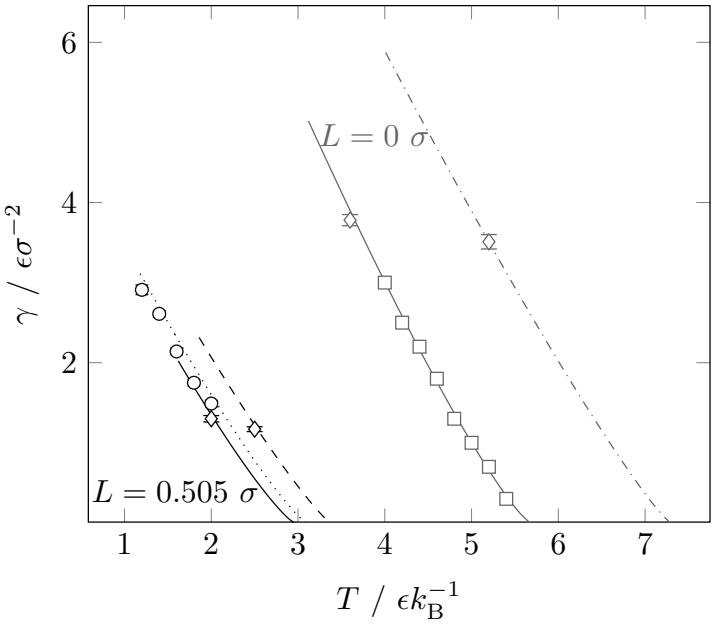

FIG. 7. Surface tension of 2CLJD fluids from the literature, including the case of the Stockmayer fluid (without elongation). The open symbols are simulation results from the literature: Enders et al.[39] (o), Mecke et al.[38] ($\diamond$) and Moore et al.[37] ($\square$). The lines represent the correlation given in Eq. (4). The line types represent the different dipole strengths: $\mu^2 = 4\ \epsilon\sigma^3$ (solid), $\mu^2 = 6\ \epsilon\sigma^3$ (dotted), $\mu^2 = 9\ \epsilon\sigma^3$ (dashed) and $\mu^2 = 12\ \epsilon\sigma^3$ (dash-dotted)

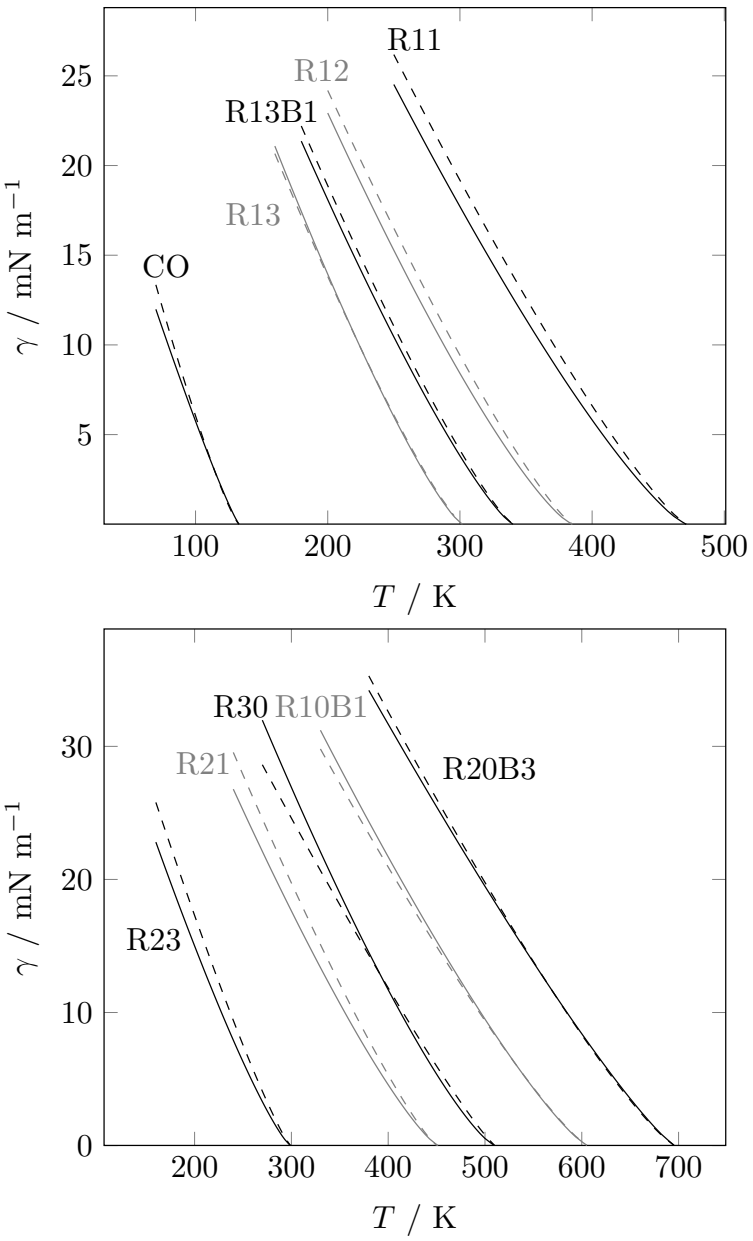

FIG. 8. Surface tension of methane derivatives and carbon monoxide over the temperature. The dashed lines are predictions based on the correlation of simulation data from the present study given in Eq. (4) and the solid lines represent DIPPR correlations[67] based on experimental data.

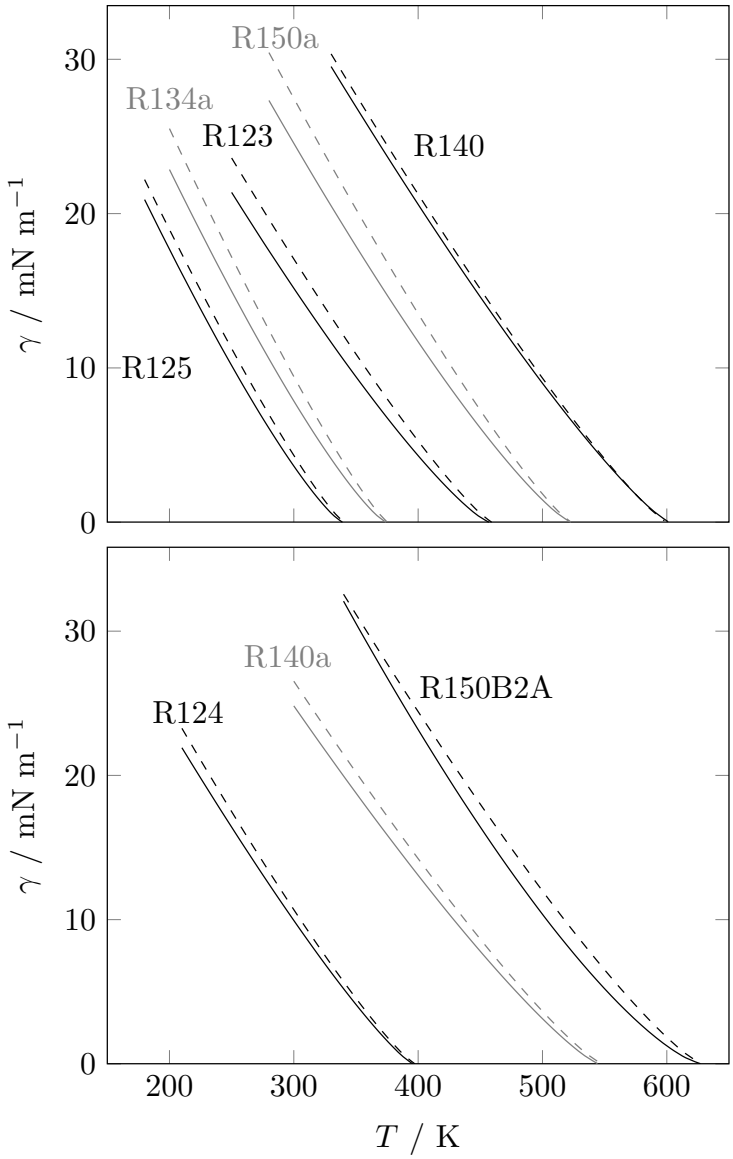

FIG. 9. Surface tension of ethane/ethene derivatives over the temperature. The dashed lines are predictions based on the correlation of simulation data from the present study given in Eq. (4) and the solid lines represent DIPPR correlations[67] based on experimental data.

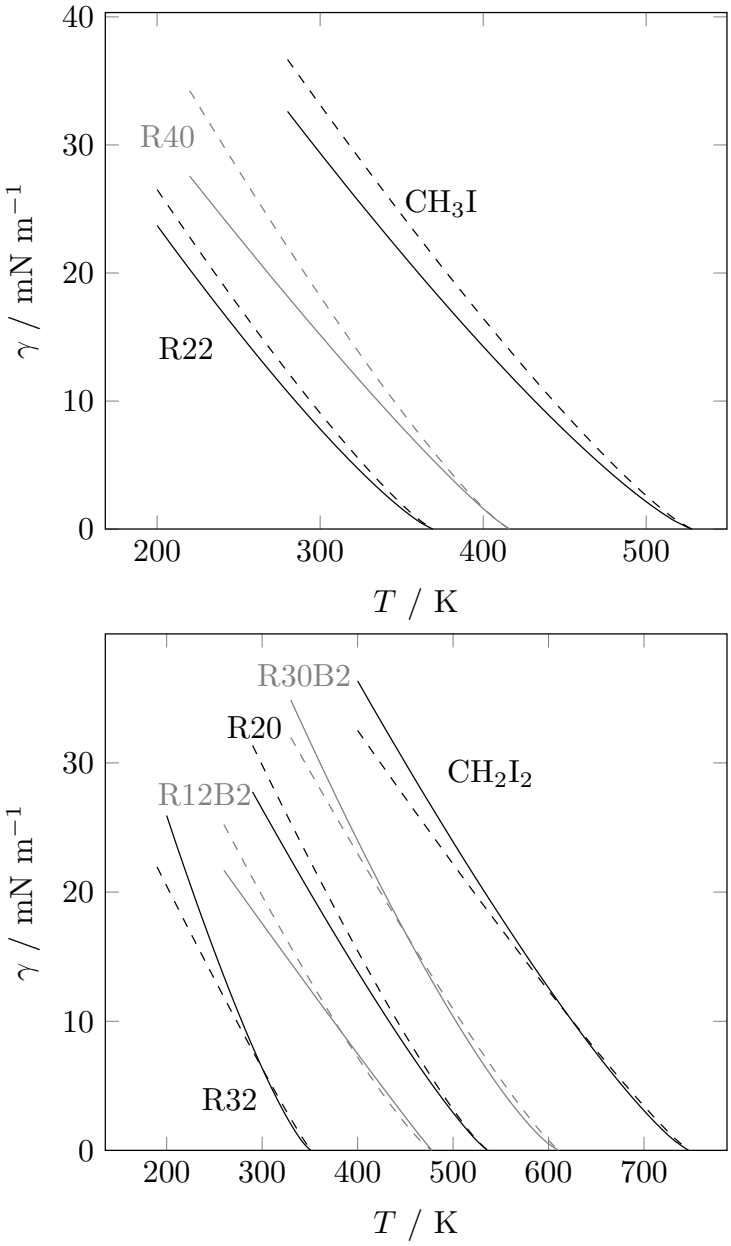

FIG. 10. Surface tension of methane derivatives over the temperature. The dashed lines are predictions based on the correlation of simulation data from the present study given in Eq. (4) and the solid lines represent DIPPR correlations[67] based on experimental data.

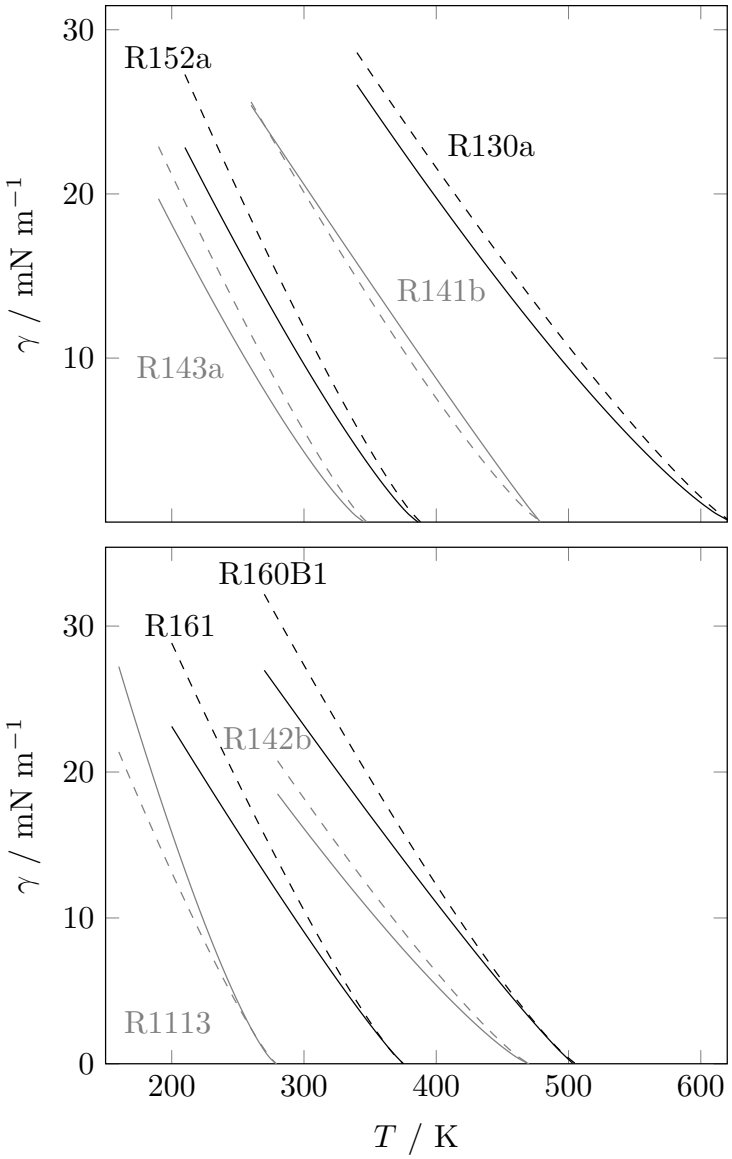

FIG. 11. Surface tension of ethane/ethene derivatives over the temperature. The dashed lines are predictions based on the correlation of simulation data from the present study given in Eq. (4) and the solid lines represent DIPPR correlations[67]. For R161 the correlation parameters from Mulero et al. are used[68]. The results for R1113 are shifted by 100K to the left and the results for R142b are shifted 60K to the right for better visibility.

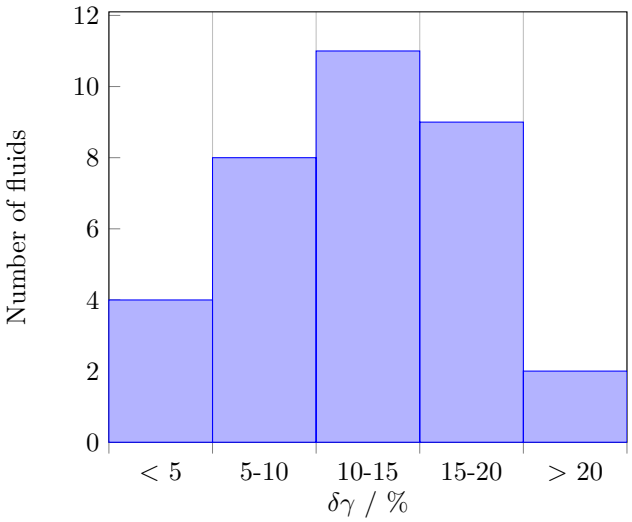

FIG. 12. Histogram of the relative deviation (temperature average between 55 and 95 % T_c) of the surface tension of 2CLJD models from correlations to experimental data[67].

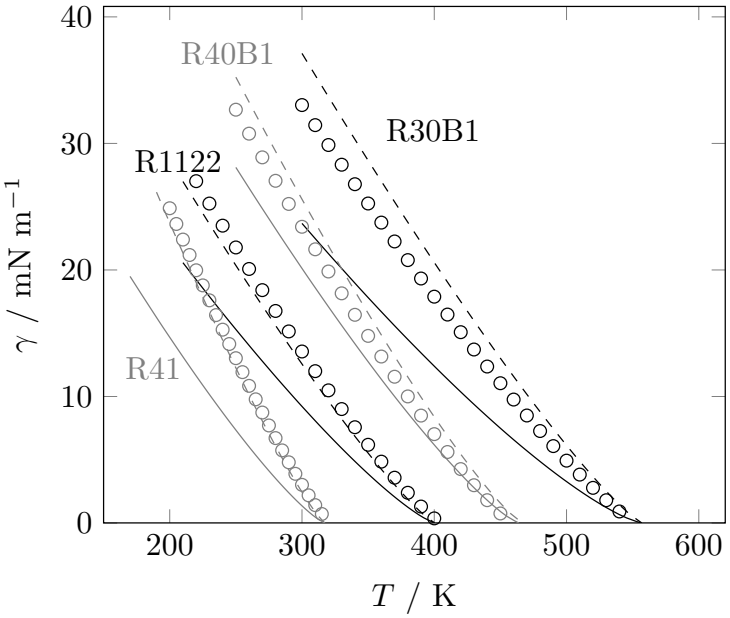

FIG. 13. Surface tension of methane and ethene derivatives over the temperature. The dashed lines are predictions based on the correlation of simulation data from the present study given in Eq. (4) and the solid lines represent DIPPR correlations[67] based on the parachor method[70,71], where the parachor was estimated based on the molecular structure[67,72]. The open symbols are predictions based on a group contribution method by Rarey et al., which is implemented in the Dortmund Data Bank[73]. No experimental data on the surface tension are available for these fluids.

TABLES

TABLE I: Simulation results for 2CLJD fluids from the present work. The numbers in parentheses indicate the uncertainties of the last decimal digits.

$L = 0\ \sigma$	$T\ /\ \epsilon k_{\mathrm{B}}^{-1}$	$p^{\mathrm{s}}\ /\ \epsilon\sigma^{-3}$	$\rho^{'}\ /\ \sigma^{-3}$	$\rho^{''}\ /\ \sigma^{-3}$	$\gamma\ /\ \epsilon\sigma^{-2}$
$\mu^2 = 0\ \epsilon\sigma^3$	3.142	0.016(1)	0.8057(1)	0.0052(5)	3.82(17)
	3.665	0.054(3)	0.7446(4)	0.0164(11)	2.62(15)
	4.189	0.135(5)	0.6741(4)	0.0399(12)	1.59(13)
	4.712	0.277(5)	0.5831(13)	0.0874(28)	0.65(6)
$\mu^2 = 3\ \epsilon\sigma^3$	3.285	0.013(2)	0.8206(3)	0.0041(7)	4.18(24)
	3.833	0.049(4)	0.7584(2)	0.0141(9)	2.92(12)
	4.380	0.129(4)	0.6870(4)	0.0360(14)	1.78(8)
	4.928	0.274(6)	0.5957(6)	0.0810(10)	0.78(11)
$\mu^2 = 6\ \epsilon\sigma^3$	3.594	0.011(1)	0.8319(1)	0.0032(4)	4.58(10)
	4.193	0.045(4)	0.7686(2)	0.0118(10)	3.29(25)
	4.792	0.125(3)	0.6957(3)	0.0320(14)	2.02(20)
	5.391	0.275(23)	0.5992(7)	0.0783(23)	0.92(13)
$\mu^2 = 9\ \epsilon\sigma^3$	3.951	0.009(1)	0.8403(1)	0.0024(3)	4.93(21)
	4.610	0.040(3)	0.7757(1)	0.0096(7)	3.50(13)
	5.268	0.117(4)	0.7016(3)	0.0272(14)	2.24(10)
	5.927	0.270(11)	0.6070(10)	0.0670(35)	1.00(9)
$\mu^2 = 12\ \epsilon\sigma^3$	4.373	0.008(2)	0.8433(1)	0.0019(5)	4.96(21)
	5.102	0.038(3)	0.7764(4)	0.0082(5)	3.72(30)
	5.831	0.116(2)	0.6992(3)	0.0248(5)	2.27(9)
	6.560	0.275(5)	0.6000(15)	0.0643(14)	1.01(9)
$\mu^2 = 16\ \epsilon\sigma^3$	4.949	0.007(2)	0.8464(5)	0.0015(2)	5.11(36)
	5.774	0.034(3)	0.7774(3)	0.0066(7)	3.92(7)
	6.599	0.111(5)	0.6968(7)	0.0213(7)	2.43(18)

	7.424	0.277(4)	0.5925(10)	0.0599(18)	1.05(14)
$\mu^2 = 20\ \epsilon\sigma^3$	5.498	0.005(1)	0.8513(5)	0.0011(2)	4.89(49)
	6.415	0.029(1)	0.7821(3)	0.0052(3)	4.09(34)
	7.331	0.098(3)	0.7002(8)	0.0171(8)	2.70(20)
	8.248	0.257(10)	0.5946(7)	0.0504(23)	1.23(18)

$L = 0.2\ \sigma$	$T\ /\ \epsilon k_{\mathrm{B}}^{-1}$	$p^{\mathrm{s}}\ /\ \epsilon\sigma^{-3}$	$\rho^{'}\ /\ \sigma^{-3}$	$\rho^{''}\ /\ \sigma^{-3}$	$\gamma\ /\ \epsilon\sigma^{-2}$
$\mu^2 = 0\ \epsilon\sigma^3$	2.588	0.011(1)	0.7116(1)	0.0044(10)	2.88(12)
	3.019	0.037(2)	0.6575(2)	0.0137(7)	2.09(8)
	3.450	0.095(4)	0.5952(2)	0.0344(15)	1.26(5)
	3.882	0.200(8)	0.5147(6)	0.0764(35)	0.54(5)
$\mu^2 = 3\ \epsilon\sigma^3$	2.713	0.010(1)	0.7218(3)	0.0037(5)	3.23(20)
	3.165	0.036(3)	0.6668(3)	0.0125(5)	2.25(19)
	3.617	0.094(7)	0.6036(4)	0.0319(21)	1.36(8)
	4.069	0.201(6)	0.5223(9)	0.0728(26)	0.60(11)
$\mu^2 = 6\ \epsilon\sigma^3$	2.950	0.007(2)	0.7307(3)	0.0026(5)	3.50(27)
	3.442	0.031(2)	0.6749(1)	0.0100(9)	2.52(12)
	3.934	0.087(3)	0.6105(1)	0.0272(7)	1.56(11)
	4.425	0.197(5)	0.5286(7)	0.0652(19)	0.71(6)
$\mu^2 = 9\ \epsilon\sigma^3$	3.229	0.007(1)	0.7368(3)	0.0021(4)	3.83(26)
	3.767	0.027(1)	0.6801(2)	0.0080(6)	2.73(16)
	4.306	0.082(3)	0.6146(3)	0.0234(6)	1.72(13)
	4.844	0.190(2)	0.5318(7)	0.0589(20)	0.78(10)
$\mu^2 = 12\ \epsilon\sigma^3$	3.567	0.006(1)	0.7381(2)	0.0017(2)	3.98(13)
	4.162	0.027(2)	0.6792(3)	0.0071(3)	2.89(21)
	4.756	0.082(3)	0.6111(6)	0.0217(10)	1.76(15)
	5.351	0.195(4)	0.5229(7)	0.0561(16)	0.77(13)
$\mu^2 = 16\ \epsilon\sigma^3$	3.992	0.004(1)	0.7434(2)	0.0012(2)	4.27(31)
	4.658	0.023(2)	0.6831(4)	0.0055(5)	3.12(17)
	5.323	0.074(3)	0.6134(3)	0.0177(6)	1.99(10)
	5.989	0.187(3)	0.5238(6)	0.0498(23)	0.85(17)

$L = 0.4\ \sigma$	$T\ /\ \epsilon k_{\mathrm{B}}^{-1}$	$p^{\mathrm{s}}\ /\ \epsilon\sigma^{-3}$	$\rho^{'}\ /\ \sigma^{-3}$	$\rho^{''}\ /\ \sigma^{-3}$	$\gamma\ /\ \epsilon\sigma^{-2}$
$\mu^2 = 0\ \epsilon\sigma^3$	1.898	0.006(1)	0.5809(1)	0.0031(5)	1.90(7)
	2.214	0.021(1)	0.5367(3)	0.0105(8)	1.36(8)
	2.530	0.055(3)	0.4857(4)	0.0265(15)	0.82(4)
	2.847	0.116(3)	0.4191(9)	0.0604(12)	0.34(6)
$\mu^2 = 3\ \epsilon\sigma^3$	1.987	0.005(1)	0.5878(2)	0.0025(3)	2.07(7)
	2.318	0.019(1)	0.5432(2)	0.0091(5)	1.45(7)
	2.649	0.053(1)	0.4916(3)	0.0243(9)	0.88(4)
	2.980	0.115(4)	0.4246(9)	0.0566(23)	0.38(6)
$\mu^2 = 6\ \epsilon\sigma^3$	2.155	0.004(1)	0.5932(2)	0.0020(3)	2.31(8)
	2.514	0.017(1)	0.5477(2)	0.0072(5)	1.61(7)
	2.873	0.049(2)	0.4952(3)	0.0209(9)	0.99(3)
	3.232	0.112(3)	0.4279(10)	0.0512(16)	0.43(10)
$\mu^2 = 9\ \epsilon\sigma^3$	2.345	0.003(1)	0.5980(2)	0.0013(2)	2.47(18)
	2.736	0.015(1)	0.5516(3)	0.0059(6)	1.79(13)
	3.127	0.044(1)	0.4984(1)	0.0175(8)	1.11(3)
	3.518	0.104(3)	0.4305(9)	0.0445(10)	0.50(7)
$\mu^2 = 12\ \epsilon\sigma^3$	2.569	0.003(0)	0.6002(3)	0.0010(2)	2.62(18)
	2.997	0.013(2)	0.5524(3)	0.0046(5)	1.90(13)
	3.426	0.042(2)	0.4973(2)	0.0153(7)	1.20(9)
	3.854	0.103(3)	0.4269(6)	0.0414(25)	0.55(9)

$L = 0.505\ \sigma$	$T\ /\ \epsilon k_{\mathrm{B}}^{-1}$	$p^{\mathrm{s}}\ /\ \epsilon\sigma^{-3}$	$\rho^{'}\ /\ \sigma^{-3}$	$\rho^{''}\ /\ \sigma^{-3}$	$\gamma\ /\ \epsilon\sigma^{-2}$
$\mu^2 = 0\ \epsilon\sigma^3$	1.641	0.004(1)	0.5292(2)	0.0025(7)	1.57(9)
	1.915	0.015(1)	0.4890(2)	0.0087(6)	1.12(7)
	2.188	0.041(1)	0.4429(3)	0.0227(9)	0.67(3)
	2.462	0.087(2)	0.3829(9)	0.0520(15)	0.29(5)
$\mu^2 = 3\ \epsilon\sigma^3$	1.723	0.003(1)	0.5343(2)	0.0020(2)	1.68(12)
	2.010	0.014(1)	0.4935(1)	0.0077(3)	1.21(2)
	2.297	0.040(1)	0.4464(4)	0.0211(14)	0.73(4)
	2.584	0.089(2)	0.3855(10)	0.0507(14)	0.32(5)
$\mu^2 = 6\ \epsilon\sigma^3$	1.860	0.003(1)	0.5396(1)	0.0015(3)	1.80(10)
	2.170	0.012(2)	0.4982(2)	0.0060(6)	1.34(6)
	2.480	0.036(2)	0.4507(3)	0.0177(7)	0.83(6)
	2.790	0.084(3)	0.3901(5)	0.0442(22)	0.36(7)
$\mu^2 = 9\ \epsilon\sigma^3$	2.026	0.002(1)	0.5431(1)	0.0011(4)	2.03(12)
	2.364	0.010(1)	0.5008(1)	0.0048(5)	1.46(3)
	2.702	0.032(2)	0.4523(2)	0.0144(9)	0.92(3)
	3.039	0.079(1)	0.3907(6)	0.0390(17)	0.43(5)
$\mu^2 = 12\ \epsilon\sigma^3$	2.206	0.002(0)	0.5462(1)	0.0008(1)	2.21(10)
	2.573	0.009(1)	0.5031(4)	0.0037(5)	1.58(15)
	2.941	0.030(2)	0.4537(2)	0.0123(7)	1.02(6)
	3.308	0.074(3)	0.3913(4)	0.0340(15)	0.49(7)

$L = 0.6\ \sigma$	$T\ /\ \epsilon k_{\mathrm{B}}^{-1}$	$p^{\mathrm{s}}\ /\ \epsilon\sigma^{-3}$	$\rho^{'}\ /\ \sigma^{-3}$	$\rho^{''}\ /\ \sigma^{-3}$	$\gamma\ /\ \epsilon\sigma^{-2}$
$\mu^2 = 0\ \epsilon\sigma^3$	1.472	0.004(4)	0.4902(1)	0.0022(4)	1.35(8)
	1.718	0.012(1)	0.4525(2)	0.0076(12)	0.93(1)
	1.963	0.033(2)	0.4091(2)	0.0205(7)	0.58(7)
	2.209	0.073(2)	0.3527(10)	0.0491(17)	0.24(4)
$\mu^2 = 3\ \epsilon\sigma^3$	1.535	0.003(1)	0.4961(1)	0.0018(3)	1.47(10)
	1.791	0.011(1)	0.4583(2)	0.0065(1)	1.02(7)
	2.046	0.031(1)	0.4148(4)	0.0184(6)	0.62(5)
	2.302	0.071(1)	0.3589(6)	0.0446(2)	0.28(5)
$\mu^2 = 6\ \epsilon\sigma^3$	1.664	0.002(0)	0.4998(1)	0.0013(2)	1.62(8)
	1.942	0.009(1)	0.4611(2)	0.0053(4)	1.12(8)
	2.219	0.029(2)	0.4165(5)	0.0157(6)	0.70(7)
	2.497	0.069(6)	0.3566(10)	0.0430(15)	0.31(7)
$\mu^2 = 9\ \epsilon\sigma^3$	1.824	0.002(0)	0.5017(1)	0.0009(1)	1.73(8)
	2.128	0.008(1)	0.4616(2)	0.0044(7)	1.24(8)
	2.432	0.027(1)	0.4155(1)	0.0137(8)	0.75(2)
	2.736	0.067(2)	0.3560(7)	0.0372(17)	0.33(6)
$\mu^2 = 12\ \epsilon\sigma^3$	1.964	0.001(0)	0.5071(3)	0.0006(1)	1.94(16)
	2.291	0.006(0)	0.4670(2)	0.0031(1)	1.39(9)
	2.618	0.022(1)	0.4213(1)	0.0105(7)	0.87(6)
	2.946	0.058(1)	0.3634(6)	0.0300(13)	0.41(4)

$L = 0.8\ \sigma$	$T\ /\ \epsilon k_{\mathrm{B}}^{-1}$	$p^{\mathrm{s}}\ /\ \epsilon\sigma^{-3}$	$\rho^{'}\ /\ \sigma^{-3}$	$\rho^{''}\ /\ \sigma^{-3}$	$\gamma\ /\ \epsilon\sigma^{-2}$
$\mu^2 = 0\ \epsilon\sigma^3$	1.229	0.002(0)	0.4304(1)	0.0017(3)	1.03(5)
	1.434	0.008(1)	0.3962(1)	0.0064(5)	0.74(8)
	1.639	0.023(1)	0.3568(3)	0.0175(7)	0.42(3)
	1.844	0.053(1)	0.3050(10)	0.0426(14)	0.17(4)
$\mu^2 = 3\ \epsilon\sigma^3$	1.276	0.001(0)	0.4360(1)	0.0012(2)	1.13(4)
	1.489	0.007(1)	0.4018(2)	0.0052(6)	0.79(3)
	1.702	0.021(1)	0.3623(3)	0.0152(5)	0.49(5)
	1.914	0.050(1)	0.3120(5)	0.0380(8)	0.22(2)
$\mu^2 = 6\ \epsilon\sigma^3$	1.390	0.001(0)	0.4389(1)	0.0010(2)	1.23(7)
	1.621	0.006(1)	0.4035(1)	0.0043(4)	0.87(4)
	1.853	0.020(1)	0.3624(3)	0.0134(6)	0.54(4)
	2.084	0.050(2)	0.3096(6)	0.0358(17)	0.22(2)
$\mu^2 = 9\ \epsilon\sigma^3$	1.512	0.001(0)	0.4431(1)	0.0007(2)	1.37(6)
	1.764	0.005(0)	0.4067(3)	0.0033(2)	0.98(5)
	2.016	0.018(1)	0.3648(3)	0.0112(7)	0.59(3)
	2.268	0.046(1)	0.3112(7)	0.0313(9)	0.26(4)
$\mu^2 = 12\ \epsilon\sigma^3$	1.628	0.001(0)	0.4495(1)	0.0005(2)	1.55(9)
	1.899	0.004(0)	0.4128(1)	0.0022(3)	1.13(6)
	2.170	0.015(1)	0.3713(2)	0.0082(5)	0.71(4)
	2.442	0.040(2)	0.3190(7)	0.0249(16)	0.33(5)

$L = 1.0\ \sigma$	$T\ /\ \epsilon k_{\mathrm{B}}^{-1}$	$p^{\mathrm{s}}\ /\ \epsilon\sigma^{-3}$	$\rho^{'}\ /\ \sigma^{-3}$	$\rho^{''}\ /\ \sigma^{-3}$	$\gamma\ /\ \epsilon\sigma^{-2}$
$\mu^2 = 0\ \epsilon\sigma^3$	1.057	0.001(0)	0.3969(1)	0.0011(1)	0.91(6)
	1.233	0.005(0)	0.3658(1)	0.0044(4)	0.65(4)
	1.410	0.015(1)	0.3303(1)	0.0128(7)	0.39(2)
	1.586	0.036(1)	0.2856(5)	0.0319(15)	0.19(3)
$\mu^2 = 3\ \epsilon\sigma^3$	1.126	0.001(0)	0.3974(2)	0.0011(3)	0.98(6)
	1.313	0.005(1)	0.3649(1)	0.0044(4)	0.66(4)
	1.501	0.017(2)	0.3272(4)	0.0135(14)	0.40(3)
	1.688	0.040(1)	0.2789(6)	0.0348(14)	0.17(3)
$\mu^2 = 6\ \epsilon\sigma^3$	1.206	0.001(0)	0.4047(1)	0.0006(2)	1.07(5)
	1.407	0.004(0)	0.3751(2)	0.0032(2)	0.76(4)
	1.608	0.014(1)	0.3338(2)	0.0104(2)	0.47(3)
	1.809	0.036(1)	0.2861(9)	0.0284(10)	0.21(5)
$\mu^2 = 9\ \epsilon\sigma^3$	1.307	0.0005(2)	0.4119(1)	0.0004(1)	1.24(8)
	1.525	0.003(0)	0.3779(2)	0.0022(2)	0.88(6)
	1.742	0.011(1)	0.3399(2)	0.0079(7)	0.55(2)
	1.960	0.032(1)	0.2934(4)	0.0238(11)	0.27(4)
$\mu^2 = 12\ \epsilon\sigma^3$	1.422	0.0002(1)	0.4188(1)	0.0002(1)	1.39(5)
	1.659	0.002(0)	0.3840(2)	0.0016(2)	1.01(2)
	1.896	0.010(1)	0.3449(1)	0.0063(5)	0.64(4)
	2.122	0.027(2)	0.2994(3)	0.0186(16)	0.32(6)

TABLE II. Parameters of the correlations for A (Eq. (5)) and B (Eq. (6)), determined from a fit to the present simulation results.

a	$1.17804 \cdot 10^{1}$	d_1	$3.48192 \cdot 10^{-1}$
b_1	-2.80758	d_2	$-2.54544 \cdot 10^{-3}$
b_2	$9.27082 \cdot 10^{-3}$	e	2.76732
c	-9.84336	f	$1.08296 \cdot 10^{-1}$
α	1.24486	β	$-8.54972 \cdot 10^{-3}$

TABLE III. Parameters of the molecular models of Stoll et al.[6]. Deviations $\delta\rho'$ and δp^{s} as given by Stoll et al.[6]. Values in brackets indicate that the deviation $\delta\gamma$ is calculated between two predictive methods and no experimental data are available.

Name	Formula	CAS RN	σ / Å	ϵ / k_{B}	L / Å	μ / D	$\delta\rho'$	δp^{s}	$\delta\gamma$
Carbon monoxide	CO	630-08-0	3.3009	36.897	1.1405	0.7378	0.38	0.29	5.8
R10B1	$CBrCl_3$	75-62-7	4.1366	305.34	3.9869	3.6313	1.03	0.26	2.5
R11	$CFCl_3$	75-69-4	4.0213	224.15	3.3377	2.7009	0.31	2.95	11.1
R12	CF_2Cl_2	75-71-8	3.8286	185.66	3.2700	2.3219	0.51	1.62	12.4
R12B1	$CBrClF_2$	353-59-3	3.8560	212.23	3.5957	2.6786	0.65	0.17	(5.0)
R12B2	CBr_2F_2	75-61-6	4.1317	198.08	2.7356	2.5137	0.47	6.69	9.3
R13	CF_3Cl	75-72-9	3.6184	145.95	3.0738	1.8261	0.55	1.66	1.5
R13B1	$CBrF_3$	75-63-8	3.6817	170.32	3.3573	2.0478	0.65	0.14	6.5
R20	$CHCl_3$	67-66-3	3.8153	265.29	3.7798	3.3920	0.29	1.31	11.3
R20B3	$CHBr_3$	75-25-2	4.0575	357.41	3.9423	3.5204	0.35	0.98	1.8
R21	$CHFCl_2$	75-43-4	3.6522	220.69	3.4396	2.7852	0.76	0.66	13.6
R22	CHF_2Cl	75-45-6	3.4682	177.43	3.1203	2.2667	0.54	2.99	15.3
R23	CHF_3	75-46-7	3.2643	123.56	2.5670	2.1607	0.55	6.13	18.3
R30	CH_2Cl_2	75-09-2	4.5106	67.360	0.0000	3.3733	0.30	7.84	7.8
R30B1	CH_2BrCl	74-97-5	3.5838	274.49	3.5662	3.1998	1.13	0.47	(72.0)
R30B2	CH_2Br_2	74-95-3	4.7376	87.758	0.0000	3.7104	0.26	10.7	7.7
Diiodomethane	CH_2I_2	75-11-6	5.0481	96.785	0.0000	4.8971	0.29	1.44	6.1
R32	CH_2F_2	75-10-5	3.8971	38.993	0.0000	2.4745	0.72	6.43	10.8
R40	CH_3Cl	74-87-3	3.3409	186.57	2.5725	2.0217	0.22	1.09	18.0
R40B1	CH_3Br	74-83-9	3.4557	213.81	2.6146	1.8536	0.15	2.54	(32.3)
Iodomethane	CH_3I	74-88-4	3.6367	232.86	2.7083	2.4983	0.14	1.11	15.9
R41	CH_3F	593-53-3	3.0382	137.64	2.4530	1.8850	0.17	1.46	(66.3)
R112a	CCl_3-CF_2Cl	76-11-9	4.3651	258.25	4.2542	4.7132	0.33	0.33	(14.3)
R123	$CHCl_2$-CF_3	306-83-2	4.0530	221.75	4.0530	3.7002	0.76	4.24	17.8
R123B1	$CHClBr$-CF_3	151-67-7	4.6727	151.78	2.0700	3.7380	0.37	0.11	(18.9)
R124	$CHFCl$-CF_3	2837-89-0	3.8852	192.25	3.8852	3.2190	0.77	5.42	8.5
R125	CHF_2-CF_3	354-33-6	3.6861	162.77	3.6861	2.8245	0.83	6.31	13.3
R130a	CH_2Cl-CCl_3	630-20-6	4.3282	292.86	4.1261	4.7919	0.52	2.82	13.6
R131b	CH_2F-CCl_3	27154-33-2	4.1262	259.97	3.8469	4.3049	0.14	0.42	(17.6)
R134a	CH_2F-CF_3	811-97-2	3.6138	175.12	3.6138	3.0214	0.73	6.45	19.9
R140	$CHCl_2$-CH_2Cl	79-00-5	4.0768	286.36	4.0095	4.2974	0.18	5.26	3.2
R140a	CCl_3-CH_3	71-55-6	4.2224	253.75	3.4898	3.5019	0.11	3.69	10.5
R141b	CH_3-$CFCl_2$	1717-00-6	4.0209	231.43	3.6015	3.1484	0.36	2.98	9.6
R142b	CH_3-CF_2Cl	75-68-3	3.8404	193.68	3.4675	2.9610	0.68	3.17	14.9
R143a	CH_3-CF_3	420-46-2	3.5960	165.04	3.5395	2.7470	0.51	1.48	24.0
R150a	$CHCl_2$-CH_3	75-34-3	3.8579	255.24	3.8135	3.5236	0.69	0.86	16.2
R150B2A	$CHBr_2$-CH_3	557-91-5	4.0234	341.29	4.0234	2.2097	0.31	6.22	15.5
R152a	CH_3-CHF_2	75-37-6	3.5168	182.01	3.3125	2.7354	0.32	3.48	24.2
R160B1	CH_2Br-CH_3	74-96-4	3.6769	255.75	3.6769	2.9425	0.72	1.42	12.2
R161	CH_2F-CH_3	353-36-6	3.3968	176.84	3.1006	2.4110	1.61	0.35	17.3
R1113	$CFCl{=}CF_2$	79-38-9	3.7438	181.71	3.5521	2.8408	0.03	2.27	14.3
R1113B1	$CFBr{=}CF_2$	598-73-2	3.8290	218.12	3.5874	2.5273	0.68	0.18	(11.4)
R1122	$CHCl{=}CF_2$	359-10-4	3.6501	193.24	3.4497	2.7449	0.61	0.42	(37.8)
R1132a	$CF_2{=}CH_2$	75-38-7	3.7848	71.963	1.4863	2.3643	0.49	0.41	(19.6)
R1140	$CHCl{=}CH_2$	75-01-4	3.6875	181.16	2.5049	2.1078	0.19	1.46	(15.1)
R1141	$CHF{=}CH_2$	75-02-5	3.3552	155.74	2.7513	1.6565	0.37	1.55	(4.1)